influx suppression of granulocytes such as mast cells and eosinophils is still unknown. Moreover, systemically administered mesenchymal stem cells, which are able to reverse bleomycin-induced fibrotic effects in the lung tissue,[10] are a possible therapeutic modality. The interaction between keloid-derived fibroblasts and mesenchymal stem cells has therefore been investigated for cell ultrastructure as well as cell proliferation, cell migration, and extracellular matrix production.

Materials and Methods

Human mesenchymal stem cells

Human mesenchymal stem cells from a single human bone marrow donor were isolated by density gradient centrifugation and strictly sorted as positive for markers such as CD105, CD166, CD29, and CD44, and negative for cell surface makers such as CD14, CD34, and CD45. Human mesenchymal stem cells were purchased from BioWhittaker Inc. (cat. no. PT-2501, Walkersville, MD) and the cryopreserved cells were thawed immediately according to the manufacturer's instructions. Two different donor-derived hMSCs, obtained from two Asian men (23 and 24 years old), were used for this study.

The cells were cultured in "basic medium" of Dulbecco's modified Eagle's medium (DMEM) containing low glucose supplemented with 10% fetal bovine serum (FBS, heat-inactivated, cat. no. 16000-044, Gibco, Invitrogen Life Technologies, Tokyo, Japan), 200 mM L-glutamine, and penicillin (100 U/mL) and streptomycin (100 μg/mL) at 37 °C in 95% humidified air and 5% CO_2. The medium was changed every 3 days until the cells were confluent, and they were then passaged up to three times. The growth characteristics during the four passages in FBS were indistinguishable. The cells were washed using 10 mL of phosphate-buffered saline (PBS) and then liberated by exposure to 0.25% trypsin/1 mM EDTA (Gibco, cat. no. 25200-056) for 3 min at 37 °C, followed by tapping of the dishes and the addition of 5 mL of culture medium. The cells were centrifuged at 400 ***g***, and then resuspended in basic medium for the following *in vitro* examinations. The other cells were stored at −70 °C until use in a solution containing 5% human serum albumin (IS Japan Co., Ltd, Saitama, Japan, cat. no. 9988) and 10% dimethylsulfoxide (Sigma-Aldrich, Tokyo, Japan, cat. no. 41641) according to the manufacturer's instructions.

Keloid-derived fibroblasts and normal dermal fibroblasts

Three different human keloid samples were used in this investigation, taken from three different Japanese male patients (17, 21 and 23 years old) after surgical excision and subsequent adjuvant electron radiation therapy. Informed consent was obtained from each patient. The tissues were divided for tissue samples and cell culture. Some tissues were fixed in ice-cold 4% paraformaldehyde solution for 3 days, embedded in paraffin, and cut into 5-μm thick sections, and some were prepared for ultra-structural analysis. Slides were stained with hematoxylin and eosin, and Toluidine blue. For cell culture, tissue excised from a keloid lesion was minced and placed on 100-mm culture plates, consisting of the same basic medium as hMSCs at 37 °C in 95% humidified air and 5% CO_2 as previously established.[2] Normally, keloid-derived fibroblasts can be observed under a phase-contrast microscope after a 2-week culture with 3-day medium change. The cells were passaged when 70–80% confluence was reached. Up to five passages from initial cell dissemination were used in this experiment.

As a control, normal human dermal fibroblasts (CCS-2511), which were obtained from two Asian men (19 and 21 years old), were cultured using an FGM Bullet kit (CCM-3130; Takara Bio Inc., Shiga, Japan), containing 500 mL of fibroblast basal medium supplemented with hFGF-2, insulin, FBS, and gentamicin/amphotericin-B (manufactured by Cambrex Corp., East Rutherford, NJ, and distributed by Asahi Technoglass Corp., Tokyo, Japan), on 100-mm culture plates at 37 °C in 95% humidified air and 5% CO_2. After 24-h incubation, the growth medium was changed to basic medium in accordance with hMSCs and keloid-derived fibroblasts. The growth medium was changed every other day until the cells were confluent, and they were then passaged up to three times. The cells were washed using 10 mL of PBS and then liberated by exposure to 0.25% trypsin/1 mM EDTA (Gibco) for 3 min at 37 °C, followed by tapping of the dishes and the addition of 5 mL of culture medium. The cells were centrifuged at 400 ***g***, and then resuspended in basic medium for the following experiments. The other cells were stored at −70 °C until used in a solution containing 5% human serum albumin (IS Japan, Co., Ltd) and 10% dimethylsulfoxide (Sigma-Aldrich) according to the manufacturer's instructions.

Cell proliferation

Cell proliferation for keloid-derived fibroblasts and normal dermal cells was determined as previously established.[11] In short, 1×10^4 cells were counted using a Beckman Coulter® Cell and Particle Counter (Beckman Coulter, Tokyo, Japan) in 24-well culture dishes after 24-h incubation in basic medium. All cells were counted in triplicate and the average value was calculated for each well. Cell death was minimal and a trypan blue cell viability assay demonstrated less than 1% nonviable cells throughout the experimental observation period in basic medium.

Dual-modified Boyden chamber cell migration assay and coculture assay

First, cell culture inserts (3.0 μm/6-well or 8.0 μm/6-well) (upper chamber) initially containing 1×10^5 hMSCs or normal dermal fibroblasts in basic medium overnight were placed on the seeded top of a 6-well plate dish (lower chamber) in the same basic medium.[12] After overnight incubation, hMSCs or normal dermal fibroblasts attached to the upper chambers were transferred onto each lower chamber, onto which each cell (human keloid-derived fibroblast cells or normal dermal fibroblasts) or medium alone (no cell) was already seeded at about 50% confluence of each 6-well

plate in basic medium. The migration activity was evaluated 16 h later by counting the number of invaded hMSCs on the reverse surfaces of 3-μm and 8-μm pore membranes, stained with Nuclear First Red (TA-060-NF) LAB Vision Corp. (Fremont, CA). The experiments were repeated in five different wells for each assay after obtaining the average values of five counts microscopically.

Some hMSCs were then used for direct coculture in basic medium for further direct analysis. In the direct coculture analysis, 1×10^5 hMSCs and 1×10^5 keloid-derived fibroblasts, or 1×10^5 hMSCs and 1×10^5 normal dermal fibroblasts were incubated for 24 h in 6-well plates and subsequently sent for electron microscopic analyses. For each group, five different cell culture plates were individually investigated.

Electron microscopy

In order to perform transmission electron microscopy, keloid tissues and basic medium containing hMSCs in 10% FBS were prefixed in half-strength Karnovsky's fixative (pH 7.2, osmolarity 1400 mOsm) buffer consisting of 2% paraformaldehyde and 2.5% glutaraldehyde in 0.1 M cacodylate buffer for 2 h, postfixed in 2% osmium tetroxide solution (pH 7.4), dehydrated using a conventional procedure and embedded in epoxy resin. The hMSCs were cultured for 4 days in basic medium of low glucose DMEM supplemented with 10% FBS and 200 mM L-glutamine, penicillin (100 U/mL) and streptomycin (100 μg/mL). The cells were first centrifuged, and then washed with PBS, and the pellets at the bottom of the tube were subsequently dissolved with fixative after washing with PBS. Embedded specimens were ultrathin-sectioned and double-stained with uranyl acetate and lead citrate. These sections were observed using a Hitachi H-7100 electron microscope (Hitachi, Tokyo, Japan) at 75 kV accelerating voltage.

Next, specimens of the cell culture insert, to which the hMSCs were attached on the reverse side, prepared for scanning electron microscopy, were dehydrated and dried by critical-point drying apparatus (HCP-2, Hitachi) for scanning electron microscopy. Specimens in a 35-mm tissue culture dish (3000-035, Iwaki, Tokyo, Japan) were dehydrated through an ethanol series and freeze-dried in t-butyl alcohol in a freeze-dryer. The dried specimens were scatter-coated with gold using an ion-coater (IB-2, Eiko Engineering, Tokyo, Japan) and observed with a scanning electron microscope (S-3500 N, Hitachi)

Western blotting

For Western blotting, extracts of 5×10^5 hMSCs and 5×10^5 keloid-derived fibroblasts, 5×10^5 hMSCs and 5×10^5 normal dermal fibroblasts, or 5×10^5 normal dermal fibroblasts and 5×10^5 keloid-derived fibroblasts, in the upper and in the lower chamber, respectively, from 8-μm pore-sized dual-chamber method, were prepared after 24-h incubation cells were lysed using celLytic-M (cat. no. C2978, Sigma-Aldrich, St. Louis, MO) with aliquots containing 20 μg as protein as measured by spectrophotometer, run on an e-pagel (ATTO Co. Ltd, Tokyo, Japan) sodium dodecyl sulfate (SDS)–polyacrylamide gel electrophoresis system (25 mM Tris, 0.1% SDS and 192 mM glycine solution). Cells for Western blotting were obtained only from each lower chamber. The gels were washed with TBST solution (20 mM Tris-HCl, pH 7.4, 0.5 M NaCl, 0.05% Tween-20) for 3 min three times in a horizontal shaker. The proteins were then transferred to Hybond-P PVDF membrane (RPN2020P, Amersham Pharmacia Biotech Inc., Piscataway, NJ) in a solution of 25 mM Tris, 20% methanol, and 192 mM glycine.

The nonspecific background was blocked with 0.2% bovine serum albumin in PBS for 1 h in a horizontal shaker. The membranes were incubated for 3 h with primary antibodies against mouse fibronectin monoclonal antibody (1 : 200 dilution, Santa Cruz Biotechnology Inc., Santa Cruz, CA, cat. no. sc-8422) or mouse monoclonal GAPDH (glyceraldehyde 3-phosphate dehydrogenase) antibody (1 : 300 dilution, Santa Cruz Biotechnology, cat. no. sc-47724), and then incubated with secondary antibodies of mouse anti-rabbit horseradish peroxidase conjugated antibody (1 : 1000 dilution; Amersham Pharmacia Biotech). The blotted membranes were washed with TBST solution after each primary or secondary antibody for 3 min three times in a horizontal shaker. After incubation with ECL Plus (Amersham Pharmacia Biotech) for 3 min, the membranes were visualized in a CCD camera-loaded chemiluminescence system for protein expression (ATTO Light Capture, cat. no. 6962). Five different samples from different tissues of each group were investigated using Western blot analyses, and the protein levels were densitometrically analyzed using a CS analyzer (ATTO). For each band, the mean of five measurements was calculated. The fibronectin expression levels were normalized against internal GAPDH expression levels of each tissue.

Statistical analysis

The cell number values are expressed as mean ± standard deviation. The data among the groups were analyzed by one-way analysis of variance followed by Scheffe's *F*-test using add-in software, Statcel, to Microsoft Excel 2000. *P*-values less than 0.05 were considered significant.

Results

Cell proliferation

The keloid-derived fibroblasts proliferated at $2.4 \pm 2.48 \times 10^4$ cells at day 1, 24 h after plating the cells, then $5.1 \pm 2.07 \times 10^4$ cells at day 2, $13.2 \pm 1.16 \times 10^4$ cells at day 3, and $11.3 \pm 1.34 \times 10^4$ cells at day 4 ($P < 0.01$).

The normal dermal fibroblasts proliferated at $3.8 \pm 1.53 \times 10^4$ cells at day 1, then $5.2 \pm 3.11 \times 10^4$ cells at day 2, $7.3 \pm 3.29 \times 10^4$ cells at day 3, and $10.7 \pm 4.58 \times 10^4$ cells at day 4 ($P < 0.01$). Both the keloid-derived fibroblasts and normal dermal fibroblasts demonstrated linear cell proliferation during the 4-day observation.

Quantitative cell migration

The hMSCs were vital and the cells were healthy throughout the experiment. When normal dermal fibroblasts were placed in the lower chambers and with 3-μm pore membranes, the hMSCs only invaded 0.4 ± 0.5 cells/field. The keloid-derived fibroblasts induced hMSC migration through 3-μm pore membranes at 6.4 ± 3.8 cells/field, while keloid-derived fibroblasts induced 2.4 ± 1.3 cells/field cell migrations of normal dermal fibroblasts. There was a significant difference in hMSC migration with 8-μm membranes. The cell migration among the hMSCs in the upper and normal fibroblasts in the lower, the hMSCs in the upper and the lower and normal dermal fibroblasts in the upper, and the keloid-derived fibroblasts in the lower were 32.0 ± 6.2, 190.6 ± 51.4, 65.2 ± 9.0 cells/field, respectively, $P < 0.01$ (Fig. 1a,b). Since the keloid-derived fibroblasts demonstrated significant cell migration, further investigation following cell–cell interaction, direct coculture between the keloid-derived fibroblasts and hMSCs, as well as keloid-derived fibroblast analysis was performed.

Electron microscopy

In the dual-cell migration assay, cell morphology in the electron microscope demonstrated the differentiation of cells, such as conspicuous nucleoli and cytoplasmic subcytomembranous fibrils with dense bodies indicating myofibroblast-like structure in some cells, and thick collagen secreted granules as well as frequent mitoses (Fig. 2). Subsequently, monolayer coculture of hMSCs and keloid-derived fibroblasts demonstrated further functional differentiation, such as collagen secretion and abundant rough endoplasmic reticulum (Fig. 3).

Western blotting and quantification of extracellular matrix

The Western blot analysis of either the hMSCs in the upper chamber or none and either normal dermal fibroblasts or keloid-derived fibroblasts in the lower chamber for 24 h demonstrated significant difference in the fibronectin expression. Normalized by internal GAPDH expression for each band, the hMSCs in the upper and normal dermal fibroblasts depicted 0.8 ± 0.2, the hMSCs in the upper and keloid-derived fibroblasts depicted 2.2 ± 0.4, and normal dermal fibroblasts in the upper and keloid-derived fibroblasts in the lower depicted 1.0 ± 0.2 relative value of fibronectin expression ($P < 0.01$, between hMSCs in the upper with normal fibroblasts in the lower and hMSCs in the upper with keloid-derived fibroblasts in the lower, and between hMSCs in the upper with keloid-derived fibroblasts in the lower and normal fibroblasts in the upper with keloid-derived fibroblasts in the lower) (Fig. 4).

Discussion

Keloid-derived fibroblasts proliferated in the basic medium of hMSCs during the 4-day observation. There was little cell apoptosis during the experimental period. The dual-chamber assay demonstrated that hMSCs significantly induced cell migration with 8-μm pore membranes when keloid-derived fibroblasts were placed in the bottom plates compared to normal dermal fibroblasts in the bottom plates. In addition, even 3-μm pores, which normally do not permit the passage of hMSCs, were able to migrate. The significant cell migration suggests that keloid-derived fibroblasts are able to induced hMSC chemoattraction toward keloid cells. Normal fibroblast failed to be chemoattracted to keloid-derived fibroblasts.

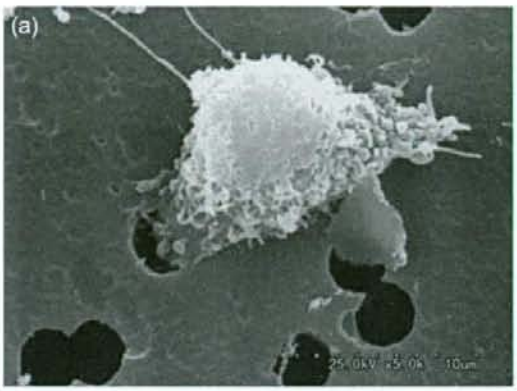

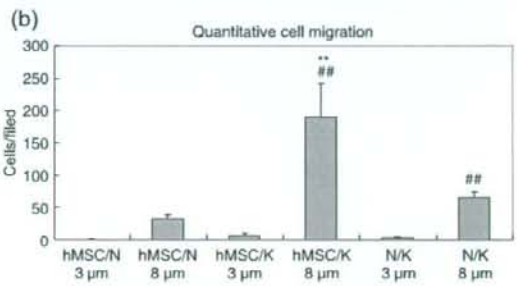

**: $P < 0.01$ to both hMSC/N 8 μm and N/K 8 μm
##: $P < 0.01$ to each 3 μm

hMSC/N: hMSCs in the upper and normal dermal fibroblasts in the lower chamber
hMSC/K: hMSCs in the upper and keloid-derived fibroblasts in the lower chamber
N/K: normal dermal fibroblasts in the upper and keloid-derived fibroblasts in the lower chamber

Figure 1 Cell migration in the reverse side of 3-μm pore membranes when keloid-derived fibroblasts were placed in the lower chamber in the dual-chamber assay. There was significant cell migration when keloid-derived fibroblasts were placed in the bottom chamber compared to when normal dermal fibroblasts ($P < 0.01$) and 8-μm pore membranes were used. hMSCs were able to pass through even 3-μm pore membranes when keloid-derived fibroblasts were used, but very few when normal dermal fibroblasts were used. More than 10-μm-diameter hMSCs were able to pass through the 3-μm diameter pores

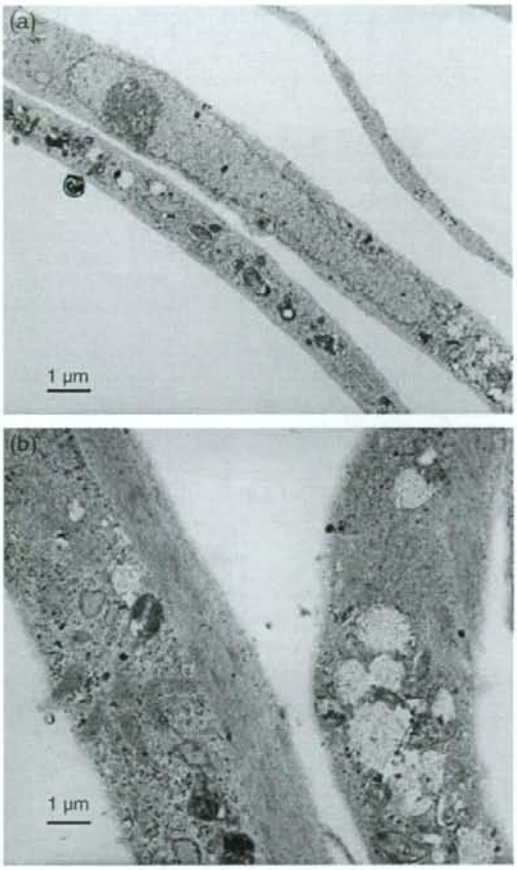

Figure 2 The ultrastructures of hMSCs when keloid-derived fibroblasts were placed in the lower chamber in the dual-chamber cell migration assay. The reverse side of transmission electron microscopy demonstrated ultrastructural differences among the treatments. (a) Conspicuous nucleoli in the elongated nuclei and microfilaments with dense bodies indicating contractive ability are found in the cell periphery. The cytoplasm developed a rough endoplasmic reticulum (×5000). (b) The high-power view demonstrated evident microfilaments with dense bodies of contractile filaments similar to those observed in myofibroblasts or smooth muscle cells (×10,000)

In the next step, to clarify either cell–cell or humoral interaction with keloid-derived fibroblasts, ultrastructural analyses with both a 3-μm pore membrane and direct monolayer coculture demonstrated hMSC cellular changes toward cell differentiation, especially cytoplasmic structural changes toward myofibroblasts. Collagen fiber bundles were expressed and secreted in the dual-chamber assay, and the cell morphology changed even more to myofibroblasts with

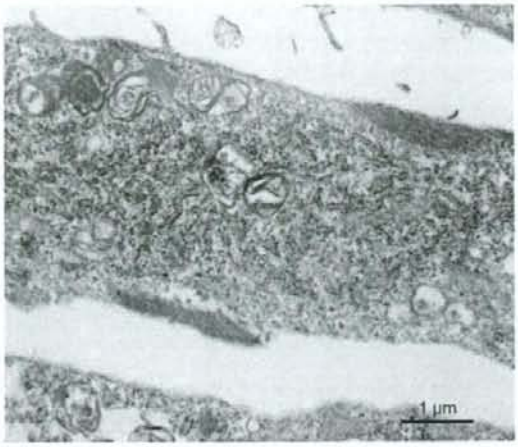

Figure 3 Monolayer coculture of hMSCs and keloid-derived fibroblasts (×10,000).The direct coculture of keloid-derived fibroblasts and hMSCs demonstrated more progressed myofibroblastic changes, characterized by cytoplasmic differentiation as depicted by abundant rough endoplasmic reticulum and the secretion of collagen-like fibers as well as actin-type microfilament bundles

abundant myofibers, rough endoplasmic reticulae and the secretion of collagen bundles. As a feature of predominant "myofibroblasts" in the keloid,[11] our data supported these characteristics as well as the invasion observed in IGF-I pathways[8] observed in the cell migration assay. Taken together, hMSCs are able to migrate into sites where keloid fibroblasts exist and may contribute to keloid pathogenesis as demonstrated by rich collagen production in the cytoplasms of hMSCs observed in both dual and direct coculture systems. The hMSCs are able to interact with other cells *in vitro* as previously demonstrated in a dual-chamber migration study,[12] and, furthermore, this study confirmed that the hMSCs are able to induce extracellular matrices when cocultured with keloid fibroblasts. In addition, this is the first evidence that keloid fibroblasts or keloid-derived humoral factors induced the hMSC differentiation although lipid mediators demonstrated the hMSC differentiation.[7] Keloid-derived fibroblasts demonstrated significantly abundant fibronectin expression with hMSCs in the upper chamber. This suggests that hMSCs participate in keloid formation by producing extracellular matrices and, thus, cause the extension and exaggeration of keloid formation. These phenomena may be implicated in the recurrence of keloids in the same area or the exacerbation of preexisting keloids through the bloodstream, since good reproducible animal models are established for the investigation of keloid recurrence and extension.

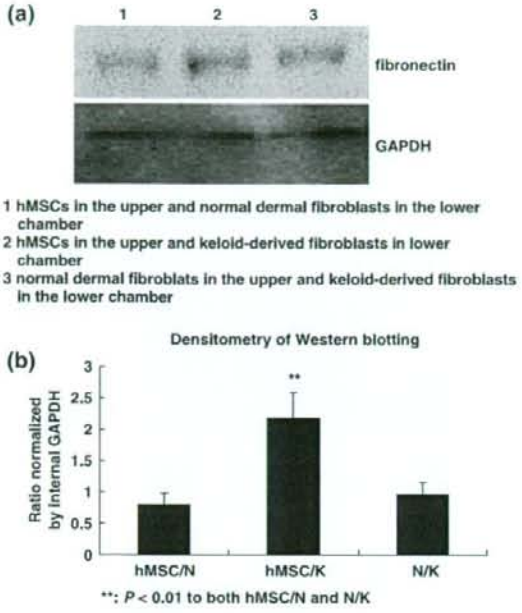

Figure 4 Fibronectin Western blot analysis from the dual-chamber incubation for 24 h. (a) Blotting demonstrated each combination of the cells (top) and internal GAPDH expression (bottom). The extracts were obtained from the bottom plates. (b) Densitometic analysis of each combination of the cells which is normalized by internal GAPDH expression. Five-time calculation of each band densitometry was statistically compared. When hMSCs were plated in the upper and keloid-derived fibroblasts in the lower chamber, there were significant differences compared to the others ($P > 0.01$)

Acknowledgment

This study was supported by grants from the Japanese Ministry of Education, Sports and Culture (nos 16390511, 16591795, 16659487, 16791091, 17659562, 17659563, 18390478, 18591967 and 18659526).

References

1 Peltonen J, Hsiao LL, Jaakkola S, *et al.* Activation of collagen gene expression in keloids: co-localization of type I and type VI collagen and transforming growth factor-β1 mRNA. *J Invest Dermatol* 1991; 97: 240–248.
2 Yoshimoto H, Ishihara H, Ohtsuru A, *et al.* Overexpression of insulin-like growth factor-1 (IGF-1) receptor and the invasiveness of cultured keloid fibroblasts. *Am J Pathol* 1999; 154: 883–889.
3 Haisa M, Okochi H, Grotendorst GR. Elevated levels of PDGFα receptors in keloid fibroblasts contribute to an enhanced response to PDGF. *J Invest Dermatol* 1994; 103: 560–563.
4 Tuan TL, Wu H, Huang EY, *et al.* Increased plasminogen activator inhibitor-1 in keloid fibroblasts may account for their elevated collagen accumulation in fibrin gel cultures. *Am J Pathol* 2003; 162: 1579–1589.
5 Rahban SR, Garner WL. Fibroproliferative scars. *Clin Plastic Surg* 2003; 30: 77–89.
6 Barry FP. Biology and clinical applications of mesenchymal stem cells. *Birth Defects Res C Embryo Today* 2003; 69: 250–256.
7 Akino K, Mineda T, Mori N, *et al.* Attenuation of cysteinyl leukotrienes induces human mesenchymal stem cell differentiation. *Wound Repair Regen* 2006; 14: 343–349.
8 Daian T, Ohtsuru A, Rogounovitch T, *et al.* Insulin-like growth factor-I enhances transforming growth factor-β-induced extracellular matrix protein production through the p38/activating transcription factor-2 signaling pathway in keloid fibroblasts. *J Invest Dermatol* 2003; 120: 956–962.
9 Yamamoto T, Takagawa S, Katayama I, *et al.* Anti-sclerotic effect of transforming growth factor-β antibody in a mouse model of bleomycin-induced scleroderma. *Clin Immunol* 1999; 92: 6–13.
10 Ortiz LA, Gambelli F, McBride C, *et al.* Mesenchymal stem cell engraftment in lung is enhanced in response to bleomycin exposure and ameliorates its fibrotic effects. *Proc Natl Acad Sci USA* 2003; 100: 8407–8411.
11 Akino K, Mineta T, Fukui M, *et al.* Bone morphogenetic protein-2 regulates proliferation of human mesenchymal stem cells. *Wound Repair Regen* 2003; 11: 354–360.
12 Akino K, Mineda T, Akita S. Early cellular changes of human mesenchymal stem cells and their interaction with other cells. *Wound Repair Regen* 2005; 13: 434–440.
13 Santucci M, Borgognoni L. Keloids and hypertrophic scars of Caucasians show distinctive morphologic and immunophenotypic profiles. *Virchows Arch* 2001; 438: 457–463.

Basic fibroblast growth factor accelerates and improves second-degree burn wound healing

Sadanori Akita, MD, PhD[1]; Kozo Akino, MD, PhD[2]; Toshifumi Imaizumi, MD[1]; Akiyoshi Hirano, MD[1]

1. Division of Plastic and Reconstructive Surgery, and
2. Division of Anatomy and Neurobiology, Department of Developmental and Reconstructive Medicine, Nagasaki University, Graduate School of Biomedical and Sciences, Nagasaki, Japan

Reprint requests:
Sadanori Akita, MD, PhD, Division of Plastic and Reconstructive Surgery, Nagasaki University, School of Medicine, 1-7-1 Sakamoto machi, Nagasaki, 852-8501, Japan.
Email: akitas@hf.rim.or.jp

Manuscript received: December 21, 2007
Accepted in final form: May 16, 2008

DOI:10.1111/j.1524-475X.2008.00414.x

ABSTRACT

Second-degree burns are sometimes a concern for shortening patient suffering time as well as the therapeutic choice. Thus, adult second-degree burn patients (average 57.8 ± 13.9 years old), mainly with deep dermal burns, were included. Patients receiving topical basic fibroblast growth factor (bFGF) or no bFGF were compared for clinical scar extent, passive scar hardness and elasticity using a Cutometer, direct scar hardness using a durometer, and moisture analysis of the stratum corneum at 1 year after complete wound healing. There was significantly faster wound healing with bFGF, as early as 2.2 ± 0.9 days from the burn injury, compared with non-bFGF use (12.0 ± 2.2 vs. 15.0 ± 2.7 days, $p < 0.01$). Clinical evaluation of Vancouver scale scores showed significant differences between bFGF-treated and non-bFGF–treated scars ($p < 0.01$). Both maximal scar extension and the ratio of scar retraction to maximal scar extension, elasticity, by Cutometer were significantly greater in bFGF-treated scars than non-bFGF–treated scars (0.23 ± 0.10 vs. 0.14 ± 0.06 mm, 0.59 ± 0.20 vs. 0.49 ± 0.15 mm: scar extension, scar elasticity, bFGF vs. non-bFGF, $p < 0.01$). The durometer reading was significantly lower in bFGF-treated scars than in non-bFGF–treated scars (16.2 ± 3.8 vs. 29.3 ± 5.1, $p < 0.01$). Transepidermal water loss, water content, and corneal thickness were significantly less in bFGF-treated than in non-bFGF–treated scars ($p < 0.01$).

Second-degree burns are sometimes a concern as to whether early surgery should be selected or whether it should be delayed until remnant dermal components are reepithelialized. Early excision and grafting of < 20% of the total burn surface area (TBSA) is superior to nonoperative treatment from the viewpoint of hypertrophic scar (HS) formation and scar quality.[1] Recently, dermal replacement template surgery on postburn day 5, followed by auto-grafting on postburn day 21 for patients with deep dermal burns to full-thickness burns were demonstrated as safe and effective treatment modalities for the TBSA, 43% burns.[2] On the other hand, a conservative approach for deep dermal burn wounds using polarized-light irradiation resulted in a shorter healing time, almost no HS, and optimal esthetic and functional outcomes with a relatively long-term follow-up.[3]

Another modality for the treatment of burn wounds, systemic administration of growth hormone, which attenuates pro-inflammatory cytokines such as tumor necrosis factor-α (TNF-α), is beneficial for the metabolism, and may lead to accelerated wound healing at donor sites in patients with large cutaneous burns.[4] Second-degree thermal injuries of rat skin showed the complement-independent involvement of pro-inflammatory cytokines such as interleukin-1 (IL-1), TNF-α, and IL-6 as results of reactive oxygen metabolites generated by neutrophils, which were accumulated in the dermal burn wounds.[5] Another heparin-binding cytokine, midkine, showed enhanced expression as early as day 1 after deep dermal burn injury in a rat model.[6] Continuous recombinant human erythropoietin from 3 hours to 14 days after deep burn injury improved angiogenesis and wound healing in a mouse model by the expression of CD31 endothelial markers and inducible nitric oxide synthases, and the wound content of nitric oxide products and by augmenting vascular endothelial growth factor content.[7] Among cytokines, basic fibroblast growth factor (bFGF) showed endogenous immunolocalization in the human dermis in partial-thickness burns from day 4 to day 11. The bFGF participates in cutaneous wound healing by activating local macrophages up to the remodeling phase, which occurs several weeks after injury.[8] The bFGF in burn wounds may be a presynthesized mediator that is released locally from injury sites, and thus may play an important role in early wound healing.[9] In adult second-degree burns, the topical application of bFGF within 5 days postinjury showed significantly better regeneration of granulation tissues and newly formed capillaries in a randomized-controlled clinical trial.[10] We therefore sought to investigate bFGF in second-degree burns with conventional wound care alone. Objective analyses using a moisture meter for healed epithelial layer (stratum corneum) function, a durometer for scar hardness, and a Cutometer for scar elasticity as well as clinical assessment were compared in bFGF-treated and non-bFGF–treated groups.

Table 1. Patient profiles

	bFGF (n=51)	non-bFGF (n=51)	Control (non-wounded) (n=51)
Sex (F:M)	24 : 27	21 : 30	25 : 26
Age (years)	60.0 ± 10.8	54.4 ± 16.3	58.9 ± 13.9
TBSA (%)	8.9 ± 4.3	9.5 ± 5.0	
Burn type	Scald=33	Scald=31	
	Flame=14	Flame=14	
	Contact=4	Contact=6	
Location			
	Total=119	Total=122	
	Upper extremity=33	Upper extremity=33	
	Lower extremity=34	Lower extremity=33	
	Torso=27	Torso=27	
	Face=25	Face=29	
Healing time (days)	12.0 ± 2.2	15.0 ± 2.7**	

Upper extremity=arm, hand, finger.
Lower extremity=thigh, leg, foot, toe.
Torsochest, back, abdomen.
**$p < 0.01$.

PATIENTS AND METHODS

Patients

We enrolled 153 subjects (22–90 years old; average 57.8 ± 13.9 years of age, 51 with bFGF treatment, 51 with non-bFGF treatment, and 51 age-matched healthy volunteers) in this investigation from November 2001 to March 2006. The bFGF treatment group included 24 female and 27 male patients with an average age of 60.0 ± 10.8 years (40–87 years old), with an average TBSA of 8.9 ± 4.3%. The non-bFGF treatment group included 21 female and 30 male patients with an average age of 54.4 ± 16.3 years (22–89 years old), with an average TBSA of 9.5 ± 5.0% after approval from the internal review board in Nagasaki University Hospital. The patients were randomized by the date of their first visits to our hospital. Patients were treated with bFGF on odd days, while patients who came on even days were included in the non-bFGF–treated group. There was no statistical significance between bFGF and non-bFGF groups in terms of age or TBSA. Other than whether using bFGF or not, all therapeutic regimens were exactly the same between the two groups. For instance, the timing of the dressing changes or use of the ointment-impregnated gauzes from the initial treatment until wound healing was identical.[11] The age-matched volunteers (25 women and 26 men) were patients who visited the hospital for complaints other than scar problems with an average age of 58.9 ± 13.9 years (26–90 years old). There were no significant differences among volunteers, bFGF, and non-bFGF groups.

All burns were diagnosed as second-degree burns. The majority of the burns were deep dermal burns and some were mixed superficial and deep dermal burns at first observed clinically. The burn types were contact (n=4), flame (n=14), and scald (n=33) in the bFGF-treated group, with a similar distribution in the non-bFGF–treated burns as contact (n=6), flame (n=14), and scald (n=31). The anatomical distributions were the face (n=25 vs. 29), torso (n=27 vs. 27), upper extremities (n=33 vs. 33), and lower extremities (n=34 vs. 33) for the bFGF-treated group vs. the non-bFGF–treated group, respectively. As some patients suffered burns at more than one anatomical location, there were 119 vs. 122 locations in bFGF-treated vs. non-bFGF–treated groups, respectively (Table 1).

Split-thickness skin grafting was required in some wounds for wound coverage. However, these locations were distant from the evaluation locations and excluded for further clinical and objective analyses. For the bFGF-treated group, initial use started at 2.2 ± 0.9 days (1–4 days, mean 2.0 days) and there were no other factor differences between the two groups other than the use or nonuse of a bFGF spray on the burn wounds. The bFGF was applied on day 1 as much as possible. However, because of careful clinical observation for the first 24 hours after the burn, especially handling of blister formation, the bFGF was started on day 2 and after. When a blister was formed after 24 hours, gentle management with removal of the internal fluid through minimal nicking and bFGF was applied for the bFGF-treated group.

bFGF (Trafermin, Fiblast Spray®) and non-bFGF treatment

Genetically recombinant bFGF (Fiblast Spray®, Kaken Pharmaceutical Co., Ltd., Tokyo, Japan) was used for spraying. The beginning of bFGF use varied from 2 to 4 days postburn injury. The concentration of bFGF was 30 μg of bFGF per 30 cm^2 area as 100 μg of freeze-dried bFGF dissolved in 1 mL of benzalkonium chloride solution, with 300 μL sprayed over a 30 cm^2 area from a 5 cm

distance, and 0.3 mL of this concentration solution was applied by this method. Ointment-impregnated gauze was applied to wounds treated with bFGF after waiting for 30 seconds. The bFGF administration continued until the wound had healed.

The non-bFGF treatment groups received only ointment-impregnated gauze without bFGF spraying. Standard procedures for stabilizing the burn wounds were applied for all cases.[11]

Scar scaling

Burns were evaluated by the senior authors (S. A., K. A., and T. I.), who evaluated others' patients in a blind fashion 1 year after complete wound healing. Scar scaling was determined using the Vancouver scar scale, which included pigmentation (0=normal, 1=hypo-pigmented, 2=mixed, 3=hyperpigmented), pliability (0=normal, 1=supple, 2=yielding, 3=firm, 4=ropes, 5=contracture), height (0=flat, 1= < 2 mm, 2=2–5 mm, 3 ≥5 mm), and vascularity (0=normal, 1=pink, 2=red, 3=purple).[12] Evaluation was confirmed by the other two authors, who are also burn specialists; therefore, each wound was assessed by four different evaluators. Parameters for each scar were obtained by averaging the individual score by four observers.

Cutometer

A Cutometer® MPA 580 (Courage+Khazaka electronic GmbH, Cologne, Germany) was used to evaluate skin elasticity parameters at 1 year after complete wound healing. The Cutometer is able to measure vertical deformation of the skin by suctioning into a round probe, 6 mm in diameter. A vacuum load of 500 mbar was used over the skin (or scar) surface for 1 second, followed by normal pressure for 1 second. Each measurement was repeated three times and the mean value of four adjacent points at least 6 mm apart and 12 mm from the intact skin was assessed at 25 °C room temperature and 50% humidity with air conditioning. As discussed and reported previously, two parameters of the Cutometer were used in this investigation. The Uf (depicted as R0) stands for the maximal skin (or scar) extension of the deformation at the end of the vacuum period; Ur/Uf (R7) stands for the ratio of the retraction (Ur) to the maximal extension (Uf) and reflects the elasticity of the measuring subjects.[13,14]

Durometer

The durometer used in this investigation was a TECLOCK GS-701N (Teclock Co. Ltd., Nagano, Japan), which follows the international standard of SRIS 0101 and is defined as a spring instrument to measure hardness, with a 5-mm-diameter round noninvasive gauge head, and a value range from 519 to 8379 mN (55–855 gf) at 1 year after complete wound healing. The measurement of each point was always perpendicular to the scars and was repeated five times immediately after touching the scar and at 30 seconds after touching, and the mean value of three adjacent points at least 6 mm apart and 12 mm from the edge of intact skin was assessed at 25 °C room temperature and 50% humidity with air conditioning, following the manufacturer's instructions. Informed consent was obtained from all patients and there were no complications or complaints due to durometer measurements. As a normal control, the skin hardness of similar-aged volunteers was investigated at similar anatomical and location points as a normal standard of measurement.

Moisture meter

A moisture meter (ASA-M2, Asahi Biomed Co. Ltd., Yokohama, Japan) was used to detect transepidermal water loss (TEWL), water level, and the thickness of the corneal keratinocyte layer of the skin, as well as the effective contact coefficient, determined by electrolytes in the corneal layer at 1 year after complete wound healing. The meter records were used to analyze the susceptibility of conductance using a low-frequency (160 Hz) alternate current and to detect conductance using a high-frequency (143 KHz) alternate current. The proposed formula is as follows:

$$\text{Skin conductance } (\mu c) = \text{effective contact coefficient } (\%) \times \text{water level } (\mu S).$$

To enable the use of all these formulary factors, both low- and high-frequency electric voltages were applied. The round probe of the hand-piece is 5 mm in diameter and detection was set 5 seconds after probe contact with the subject to stabilize electrodes and the skin condition. Each contact point was always perpendicular to the subject and was repeated five times, and the mean value of adjacent points at least 10 mm apart and 20 mm from the intact edge was assessed at 25 °C and 50% humidity with air conditioning, following the manufacturer's instructions. All data were immediately transferred to a personal computer for further analyses. Informed consent was obtained from all patients and there were no complications or complaints due to moisture meter measurements. The measurements were performed 1 year after compete wound healing. For moisture meter analysis, the same anatomical and location areas of bFGF-treated and non-bFGF–treated groups were compared, while skin moisture meter data of similar age-matched volunteers were investigated as a normal standard of measurement.

Statistics

The results are expressed as the mean ± standard deviation. Data between groups were evaluated by one-way analysis of variance with Bonferroni's multiple comparison procedure, and p-values < 0.05 were considered statistically significant.

RESULTS

Clinical outcome

The average healing time in the bFGF-treated and non-bFGF–treated groups was 12.0 ± 2.2 days (8–17 days) and 15.0 ± 2.7 days (11–21 days), respectively ($p < 0.01$). The scar was assessed at 1 year after complete healing.

There were 119 and 122 locations in the bFGF-treated and non-bFGF–treated groups, respectively, and postoperative HSs were clinically observed in none of 25 vs. 2 of

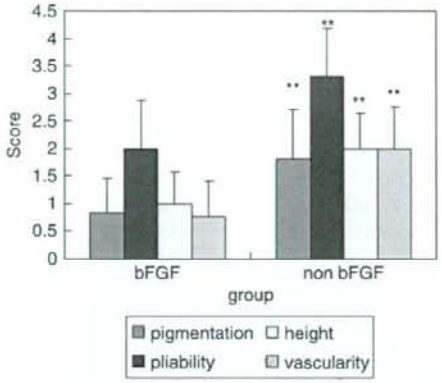

Figure 1. Vancouver scar scale. Four independent specialists evaluated at 1 year after complete wound healing. The results yielded 0.8 ± 0.6 vs. 1.8 ± 0.9, 2.0 ± 0.9 vs. 3.3 ± 0.9, 1.0 ± 0.6 vs. 2.0 ± 0.6, and 0.8 ± 0.7 vs. 2.0 ± 0.8; conventional vs. bFGF-treated, pigmentation, pliability, height, vascularity, respectively ($p < 0.01$). bFGF, basic fibroblast growth factor.

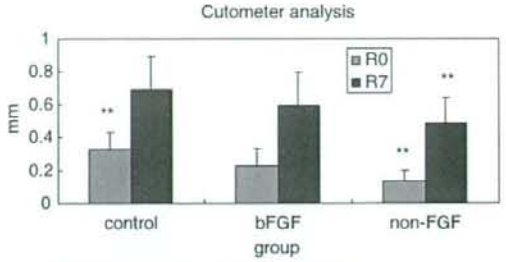

**; P<0.01, compared to bFGF group
R0; skin (scar) maximal extension
R7; skin (scar) ratio of retraction to maximal extension

Figure 2. Cutometer analysis. A Cutometer showed passive skin (scar) hardness and elasticity at 1 year after complete wound healing. The value of the maximal skin (scar) extension (denoted by R0) was significantly smaller in non-bFGF–treated scars than bFGF-treated scars and the control in the order, 0.33 ± 0.10, 0.23 ± 0.10, 0.14 ± 0.06 mm; control, bFGF-treated, non-bFGF–treated, respectively, $p < 0.01$. The skin (scar) ratio of retraction to maximal extension (denoted by R7), elasticity, was significantly smaller for non-bFGF–treated scars than bFGF-treated scars (0.69 ± 0.20, 0.59 ± 0.20, 0.49 ± 0.15 mm; control, bFGF-treated scar, non-bFGF–treated scar, respectively, $p < 0.01$). bFGF, basic fibroblast growth factor.

29 on the face, 1 of 27 vs. 3 of 27 on the torso, 1 of 33 vs. 5 of 33 on the upper extremities, and 1 of 34 vs. 4 of 33 on the lower extremities in the bFGF-treated vs. non-bFGF–treated group, respectively. The overall rate of HS formation was 2.5% for the bFGF-treated group and 11.5% for the non-bFGF–treated group. In small areas, skin grafting (< 1% of TBSA for each wound) was applied to 3 of 27 vs. 4 of 27 wounds of the torso, and 2 of 34 vs. 2 of 33 wounds on the lower extremity in the bFGF-treated and non-bFGF–treated groups, respectively. However, no HSs were observed in any location of either group at 1 year after complete wound healing and no evaluation was attempted over resurfaced scars after skin grafting.

Clinical evaluation of pigmentation, pliability, height, and vascularity showed significant differences between bFGF-treated and non-bFGF–treated scars (0.8 ± 0.6 vs. 1.8 ± 0.9, 2.0 ± 0.9 vs. 3.3 ± 0.9, 1.0 ± 0.6 vs. 2.0 ± 0.6, 0.8 ± 0.7 vs. 2.0 ± 0.8; conventional vs. bFGF-treated, pigmentation, pliability, height, vascularity, respectively, $p < 0.01$) (Figure 1). Detailed analysis of each burn location in the two groups did not show significant differences on the Vancouver scale parameter.

The bFGF was clinically permitted for use in Japan from 2001.

Skin or scar analysis by Cutometer

The values representing skin extension as R0 were significantly greater in control, nonwounded skin, followed by bFGF-treated scar, and the lowest in the non-bFGF–treated scar (0.33 ± 0.10, 0.23 ± 0.10, 0.14 ± 0.06 mm; control, bFGF-treated scar, non-bFGF–treated scar, respectively, $p < 0.01$). The relative retraction of extension, elasticity, depicted as R7, was also significantly greater in the control, followed by the bFGF-treated scar, and the lowest in the non-bFGF–treated scar (0.69 ± 0.20, 0.59 ± 0.20, 0.49 ± 0.15 mm; control, bFGF-treated scar, non-bFGF–treated scar, respectively, $p < 0.01$) (Figure 2).

Skin or scar hardness by durometer

Skin hardness measured using a durometer showed significant differences among groups. The relative value of the actual durometer reading was the lowest in the control group, which is nonwounded skin. The bFGF-treated scar was the next lowest and the non-bFGF–treated scar showed the highest value (8.0 ± 1.8, 16.2 ± 3.8, 29.3 ± 5.1; control, bFGF, non-bFGF, respectively, $p < 0.01$) (Figure 3).

Skin or scar moisture analysis

For moisture meter analyses, the effective contact coefficient was significantly higher than the nonwounded skin value (control) in both bFGF and non-bFGF–treated groups, and there was a significant difference between bFGF-treated and non-bFGF–treated groups ($10.9 \pm 1.5\%$, $18.5 \pm 1.8\%$, $4.8 \pm 1.3\%$; bFGF, non-bFGF, and nonwounded skin (control) groups, respectively, $p < 0.01$). TEWL in the bFGF-treated group was significantly less than that in the non-bFGF group (12.9 ± 2.0, $22.1 \pm 3.5\,g/m^2/hours$; bFGF-treated scar, non-bFGF–treated scar, respectively, $p < 0.01$). The bFGF-treated group showed a significantly higher TEWL value than the control (12.9 ± 2.0, $6.2 \pm 1.2\,g/m^2/hours$; bFGF-treated scar, control, respectively, $p < 0.01$). The correlation between the effective contact coefficient and

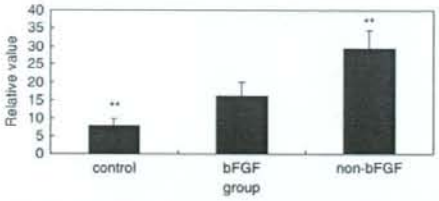

Figure 3. Durometer analysis. Direct skin (scar) hardness was obtained using a durometer at 1 year after complete wound healing. The relative value of the actual durometer reading was the lowest in the control group, which is nonwounded skin. The bFGF-treated scar was the next lowest and the non-bFGF–treated scar demonstrated the highest value (8.0 ± 1.8, 16.2 ± 3.8, 29.3 ± 5.1; control, bFGF, non-bFGF, respectively, $p < 0.01$). bFGF, basic fibroblast growth factor.

TEWL showed a significant correlation between the two ($y=0.75x+1.19$, $r^2=0.89$, $p < 0.01$).

The water content in the non-bFGF group was significantly greater than in bFGF-treated and control groups, while there was no significant difference between bFGF-treated and control groups (24.7 ± 4.5, 44.8 ± 4.9, $23.7 \pm 4.3\,\mu S$; bFGF-treated, non-bFGF–treated, control groups, respectively, $p < 0.01$; between control and non-bFGF–treated groups and between bFGF-treated and non-bFGF–treated groups). The thickness of the non-bFGF–treated group was significantly greater than both the control and the bFGF-treated groups (11.9 ± 3.0, 17.9 ± 1.7, $10.2 \pm 1.5\,\mu m$; bFGF-treated, non-bFGF–treated, control groups, respectively, $p < 0.01$; between control and non-bFGF–treated groups and between bFGF-treated and non-bFGF–treated groups) (Figure 4).

Anatomical locations of the moisture meter and the measurement conditions were similar among the three groups.

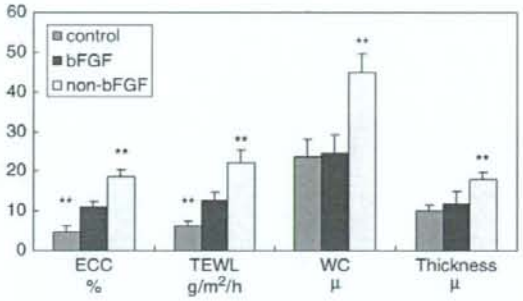

Figure 4. Moisture meter analysis. A moisture meter was used at 1 year after complete wound healing. The effective contact coefficient was significantly higher than the nonwounded skin value (control) in both bFGF-treated and non-bFGF–treated groups, and there was a significant difference between bFGF-treated and non-bFGF–treated groups ($10.9 \pm 1.5\%$, $18.5 \pm 1.8\%$, $4.8 \pm 1.3\%$; bFGF, non-bFGF, and nonwounded skin [control] groups, respectively, $p < 0.01$). Transepidermal water loss (TEWL) in control and bFGF-treated groups was significantly less than in the non-bFGF group (6.2 ± 1.2, 12.9 ± 2.0, $22.1 \pm 3.5\,g/m^2/hours$; control, bFGF-treated scar, non-bFGF–treated scar, respectively, $p < 0.01$). The water content in the non-bFGF group was significantly greater than in the bFGF-treated and control groups, while there was no significant difference between bFGF-treated and control groups (24.7 ± 4.5, 44.8 ± 4.9, $23.7 \pm 4.3\,\mu S$; bFGF-treated, non-bFGF–treated, control groups, respectively, $p < 0.01$; between control and non-bFGF–treated groups and between bFGF-treated and non-bFGF–treated groups). The thickness of the non-bFGF–treated group was significantly greater than both the control and the bFGF-treated groups (11.9 ± 3.0, 17.9 ± 1.7, $10.2 \pm 1.5\,\mu m$; bFGF-treated, non-bFGF–treated, control groups, respectively, $p < 0.01$; between control and non-bFGF–treated groups and between bFGF-treated and non-bFGF–treated groups). bFGF, basic fibroblast growth factor.

DISCUSSION

Fibroblast growth factors (FGFs) play important roles in tissue repair. Among FGFs, FGF-2 or bFGF contributes to reepithelialization and collagen deposition in a "knockout" mouse model. Further, bFGF is also involved in neuronal protection and repairs ischemic, metabolic, or traumatic brain injury.[15]

Pretreatment evaluation of second-degree burns or the depth of dermal injuries is sometimes a clinical concern[16]; however, mostly deep dermal burns in this investigation were included, as diagnosed by four burn and scar specialists, and the clinical course followed; although more precise, easy, and objective assessment methods may be further required for generalizing deep dermal "second-degree" burns using a reproducible method.[17,18]

Our therapeutic regimens of bFGF treatment for the second-degree burns in this investigation started as early as on arrival day of postburn, and burn wound healing was completed at 12 days for the bFGF-treated group; this may be compatible with the endogenous bFGF expressions observed during day 4 to day 11 as observed in rats immunohistochemically.[8]

Burn-wounded human skin obtained 2–4 weeks after wounding showed FGF receptor (FGFR)-1 and -3 expressions in basal and supra-basal layers of the epidermis as well as granulation tissues such as neo-capillaries, fibroblasts/myofibroblasts, and inflammatory cells. Thus, the bFGF and its receptor signaling pathway as well as bFGF expressed in the dermal extracellular matrix may contribute to promoting reepithelialization during the wound-healing process.[19]

The quality of the scar or the quality of wound healing should be determined after the completion of wound healing.

Clinical multiple-investigator evaluations of burn scars in the bFGF-treated group by the Vancouver scar scale were significantly improved in all parameters compared with non-bFGF–treated scars. The ratio of each parameter of pigmentation, pliability, height, and vascularity was 1 : 2.25, 1.165, 1 : 2, and 1 : 2.5: bFGF-treated scar : non-bFGF–treated scar, respectively. These data were comparable to pediatric second-degree burn scars, which were 1 : 2.43, 1 : 2.18, 1.6, and 1 : 2.38: bFGF-treated : non-bFGF–treated, respectively.[20] Previous use of a durometer

for scar hardness in post–split-thickness skin grafting showed significant improvement in association with clinical skin hardness.[21] In this investigation, another objective tool of scar quality, a Cutometer, used for passive scar extension and relative retraction to the extended scar, which reflects the elasticity of the scar, showed significant improvement in bFGF-treated second-degree, most deep dermal, burns.

Additional studies using a moisture meter enabled the evaluation of corneal layer (stratum corneum) functions by the effective contact coefficient, together with TEWL, water content, and layer thickness. Abnormal functioning of corneal layers is well demonstrated in atopic dry skin studies by increased TEWL, decreased water content, and increased thickness as seen in atopic dry skin, which is thickened. As atopic skin decreases the amount of intercellular phospholipids or ceramides, this may account for the damaged function of the corneal layers.[22]

The epidermis regulates the collagen I synthesis by dermal fibroblasts and bFGF and insulin-like growth factor increased collagen production by increasing the fibroblast cell number both in monoculture and in coculture with keratinocytes.[23] In wounded skin, especially deeper wounds, HSs and keloids showed high TEWL and water content values. These data also suggest that proliferative changes in the dermis may affect the corneal layers. As one possible mechanism, especially in keloids and HSs, complex epithelial–mesenchymal interactions may modulate transforming growth factor-β (TGF-β), which may be one of the core pathogenic factors for keloids, and keloid-derived keratinocytes highly activated TGF-β expression levels in a paracrine fashion.[24]

TGF-β is expressed in the experimental burn model, although the expression pattern fluctuated during the first 15 days after the deep dermal burn as well as other cytokines such as bFGF, IL-1, and nerve growth factor (NGF).[25]

In rats, liposomal gene transfer of keratinocyte growth factor improved wound healing and altered local immunohistochemical expression by decreasing TGF-β but by increasing FGF expression at the wound edge and under the wound bed, although the burn type was extensive with TBSA 30% and third degree.[26] This suggests that local bFGF may change the TGF-β expression pattern and thus may not lead to excessive collagen deposition as observed in HSs or keloids under certain conditions.

The bFGF-treated scars may have a better process of skin remodeling, which may avoid the subsequent development of fibro-proliferative disorders.[27] As the frequency of tape-stripping increases, water-holding defects of the corneal layers (stratum corneum) are associated with a higher value of TEWL.[28] Thus, TEWL is an important marker of hydration for epithelialization or re-epithelialization after healing. The effective contact coefficient is affected by skin surface electrolytes such as sweating; however, this value also reflects the barrier function of the skin. In our study, there was a correlation between the effective contact coefficient and TEWL. The thickness of both control nonwounded skin and bFGF-treated scars was significantly less than non-bFGF scars.

The use of bFGF for second-degree burns accelerates wound healing and improves the quality of scars by objective measurement of scar quality as well as multiple-investigator subjective evaluations.

ACKNOWLEDGMENTS

This study was supported by grants from the Japanese Ministry of Education, Sports and Culture, #18390478, 18591967, 18659526, and 19406029.

REFERENCES

1. Engrav LH, Heimbach DM, Reus JL, Harnar TJ, Marvin JA. Early excision and grafting vs. non-operative treatment of burns of interminant depth: a randomized prospective study. *J Trauma* 1983; 23: 1001–4.
2. Muangman P, Deubner H, Honari S, Heimbach DM, Engrav LH, Klein MB, Gibran NS. Correlation of clinical outcome of integra application with microbiologic and pathological biopsies. *J Trauma* 2006; 61: 1212–7.
3. Monstrey S, Hoeksema H, Saelens H, Depuydt K, Hamdi M, Van Landuyt K, Blondeel P. A conservative approach for deep dermal burn wounds using polarized-light therapy. *Br J Plast Surg* 2002; 55: 420–6.
4. Herndon DN, Hawkins HK, Nguyen TT, Pierre E, Cox R, Barrow RE. Characterization of growth hormone enhanced donor site healing in patients with large cutaneous burns. *Ann Surg* 1995; 221: 649–56.
5. Ravage ZB, Gomez HF, Czermak BJ, Watkins SA, Till GO. Mediators of microvascular injury in dermal burn wounds. *Inflammation* 1998; 22: 619–29.
6. Iwashita N, Muramatsu H, Toriyama K, Torii S, Muramatsu T. Expression of midkine in normal and burn sites of rat skin. *Burns* 1999; 25: 119–24.
7. Galeano M, Altavilla D, Bitto A, Minutoli L, Calò M, Lo Cascio P, Polito F, Giugliano G, Squadrito G, Mioni C, Giuliani D, Venuti FS, Squadrito F. Recombinant human erythropoietin improves angiogenesis and wound healing in experimental burn wounds. *Crit Care Med* 2006; 34: 1139–46.
8. Kibe Y, Takenaka H, Kishimoto S. Spatial and temporal expression of basic fibroblast growth factor protein during wound healing of rat skin. *Br J Dermatol* 2000; 143: 720–7.
9. Gibran NS, Isik FF, Heimbach DM, Gordon D. Basic fibroblast growth factor in the early human burn wound. *J Surg Res* 1994; 56: 226–34.
10. Fu X, Shen Z, Chen Y, Xie J, Guo Z, Zhang M, Sheng Z. Randomised placebo-controlled trial of use of topical recombinant bovine basic fibroblast growth factor for second-degree burns. *Lancet* 1998; 352: 1661–4.
11. Fujii T. Local treatment for extensive deep dermal thickness burn and follow-up study. *Acta Chir Plast* 1990; 32: 46–56.
12. Baryza MJ, Baryza GA. The Vancouver scar scale: an administration tool and its interrater reliability. *J Burn Care Rehabil* 1995; 16: 535–8.
13. Draaijers LJ, Botman YA, Tempelman FR, Kreis RW, Middelkoop E, van Zuijlen PP. Skin elasticity meter or subjective evaluation in scars: a reliability assessment. *Burns* 2004; 30: 109–14.
14. Morita A, Kobayashi K, Isomura I, Tsuji T, Krutmann J. Ultraviolet A1 (340–400 nm) phototherapy for scleroderma in systemic sclerosis. *J Am Acad Dermatol* 2000; 43: 670–4.

15. Steiling H, Werner S. Fibroblast growth factors: key players in epithelial morphogenesis, repair and cytoprotection. *Curr Opin Biotechnol* 2003; 14: 533–7.
16. Dunkin CS, Pleat JM, Gillespie PH, Tyler MP, Roberts AH, McGrouther DA. Scarring occurs at a critical depth of skin injury: precise measurement in a graduated dermal scratch in human volunteers. *Plast Reconstr Surg* 2007; 119: 1722–32.
17. Sheridan RL, Schomaker KT, Lucchina LC, Hurley J, Yin LM, Tompkins RG, Jerath M, Torri A, Greaves KW, Bua DP. Burn depth estimation by use of indocyanine green fluorescence: initial human trial. *J Burn Care Rehabil* 1995; 16: 602–4.
18. Pape SA, Skouras CA, Byrne PO. An audit of the use of laser Doppler imaging (LDI) in the assessment of burns of intermediate depth. *Burns* 2001; 27: 233–9.
19. Takenaka H, Yasuno H, Kishimoto S. Immunolocalization of fibroblast growth factor receptors in normal and wounded human skin. *Arch Dermatol Res* 2002; 294: 331–8.
20. Akita S, Akino K, Imaizumi T, Tanaka K, Anraku K, Yano H, Hirano A. The quality of pediatric burn scars is improved by early administration of basic fibroblast growth factor. *J Burn Care Res* 2006; 27: 333–8.
21. Akita S, Akino K, Imaizumi T, Hirano A. A basic fibroblast growth factor improved the quality of skin grafting in burn patients. *Burns* 2005; 31: 855–8.
22. Imokawa G, Abe A, Jin K, Higaki Y, Kawashima M, Hidano A. Decrease level of ceramides in stratum corneum of atopic dermatitis. *J Invest Dermatol* 1991; 96: 523–6.
23. Harrison CA, Gossiel F, Bullock AJ, Sun T, Blumsohn A, MacNeil S. Investigation of kertinocyte regulation of collagen I synthesis by dermal fibroblasts in a simple in vitro model. *Br J Dermatol* 2006; 154: 401–10.
24. Suetake T, Sasai S, Zhen YX, Ohi T, Tagami H. Functional analyses of the stratum corneum in scars. Sequential studies after injury and comparison among keloids, hypertrophic scars, and atrophic scars. *Arch Dermatol* 1996; 132: 1453–8.
25. Jurjus A, Atiyeh BS, Abdallah IM, Jurjus RA, Hayek SN, Jaoude MA, Gerges A, Tohme RA. Pharmacological modulation of wound healing in experimental burns. *Burns* 2007; 33: 892–907.
26. Pereira CT, Herndon DN, Rocker R, Jeschke MG. Liposomal gene transfer of keratinocyte growth factor improves wound healing by altering growth factor and collagen expression. *J Surg Res* 2007; 139: 222–8.
27. Rahban SR, Garner WL. Fibroproliferative scars. *Clin Plast Surg* 2003; 30: 77–89.
28. Tagami H, Yoshikuni K. Interrelationship between water-barrier and reservoir functions of pathologic stratum corneum. *Arch Dermatol* 1985; 121: 642–5.

Brain Tumor Pathol (2008) 25:97–101
DOI 10.1007/s10014-008-0238-4

CASE REPORT

Ichiro Takumi · Osamu Mori · Nobuhide Mizutani
Masataka Akimoto · Shiro Kobayashi · Akira Teramoto

Expansile neurenteric cyst arising in the frontal lobe associated with status epilepticus: report of a case and discussion of epileptogenesis

Received: July 2, 2008 / Accepted: August 19, 2008

Abstract The case of a 32-year-old Japanese man with an expansile supratentorial neurenteric cyst is described. The initial MRI revealed a left frontal extraaxial mass lesion 20 mm in diameter that showed marked expansion to 32 mm and change in its signal intensity 13 months later. Fifteen months after his visit, the patient fell into status epilepticus and underwent surgery. The cyst wall was excised, and the cyst content was totally removed. The cytology of the cystic content and pathological findings of the cyst wall were compatible with the diagnosis of neurenteric cyst. Our literature search revealed that in 86% of the patients with this lesion, the lesion was involved in the occurrence of epilepsy during the perioperative period. When a neurenteric cyst is diagnosed, shunt surgery should be avoided to prevent migrating spread of neurenteric cells.

Key words Neurenteric cyst · Status epilepticus · Enlargement

I. Takumi (✉) · N. Mizutani · S. Kobayashi
Department of Neurosurgery, Neurological Institute, Chiba Hokuso Hospital, Nippon Medical School, 1715 Kamagari, Inba, Chiba 270-1694, Japan
Tel. +81-476-99-1111; Fax +81-476-99-1906
e-mail: takumi@nms.ac.jp

O. Mori
Department of Pathology, Chiba Hokuso Hospital, Nippon Medical School, Chiba, Japan

M. Akimoto
Department of Plastic Surgery, Chiba Hokuso Hospital, Nippon Medical School, Chiba, Japan

A. Teramoto
Department of Neurosurgery, Nippon Medical School, Tokyo, Japan

Part of this work was presented at the 24th annual meeting of the Japanese Society for Brain Tumor Pathology on June 29, 2006, in Okinawa, Japan. This work was supported by a grant (to I.T.) from the Education and Research Software Updating Program of the Promotion an Mutual Aid Corporation for Private Schools of Japan.

Introduction

When a supratentorial cystic lesion with cerebral cortex involvement is detected, the next radiologic step is to see whether there is enhancement by computed tomography/magnetic resonance imaging (CT/MRI), or thinning of the calvarium, as the enhancement suggests malignancy and the latter an arachnoid cyst. If the lesion is an extraaxial mass, however, various central nervous system (CNS)- and non-CNS-derived cysts should be considered for the differential diagnosis. Neurenteric cyst, a non-CNS-derived lesion, is known by several alternative terms such as enterogenous cyst, endodermal cyst, foregut cyst, epithelial cyst, bronchogenic cyst, and respiratory cyst. These terms reflect the pathological and etiological features of this lesion, which arises from the endoderm.[1] A neurenteric cyst contains proteins at various concentrations;[1] however, MRI signal analysis of the cyst components does not by itself lead to the diagnosis of the lesion. All the recently reported neurenteric cysts were diagnosed only after resection, by immunohistochemistry and electron microscopy. Further, most previously reported neurenteric cysts showed spinal involvement. Supratentorial neurenteric cysts are difficult to diagnose preoperatively.

According to our search of the literature, one of the features of supratentorial neurenteric cysts located in the cerebral cortex is their association with epilepsy. We encountered a patient with this rare lesion that had arisen in the frontal lobe and was characterized by both its expansility and status epilepticus.

Case report

The patient was a 32-year-old Japanese man who was initially referred to our outpatient clinic for further evaluation and treatment of persistent headache. The patient had no history of infection, trauma, hemorrhage, tumor, or epilepsy. MRI revealed a left frontal mass of T_1 hypo- and T_2

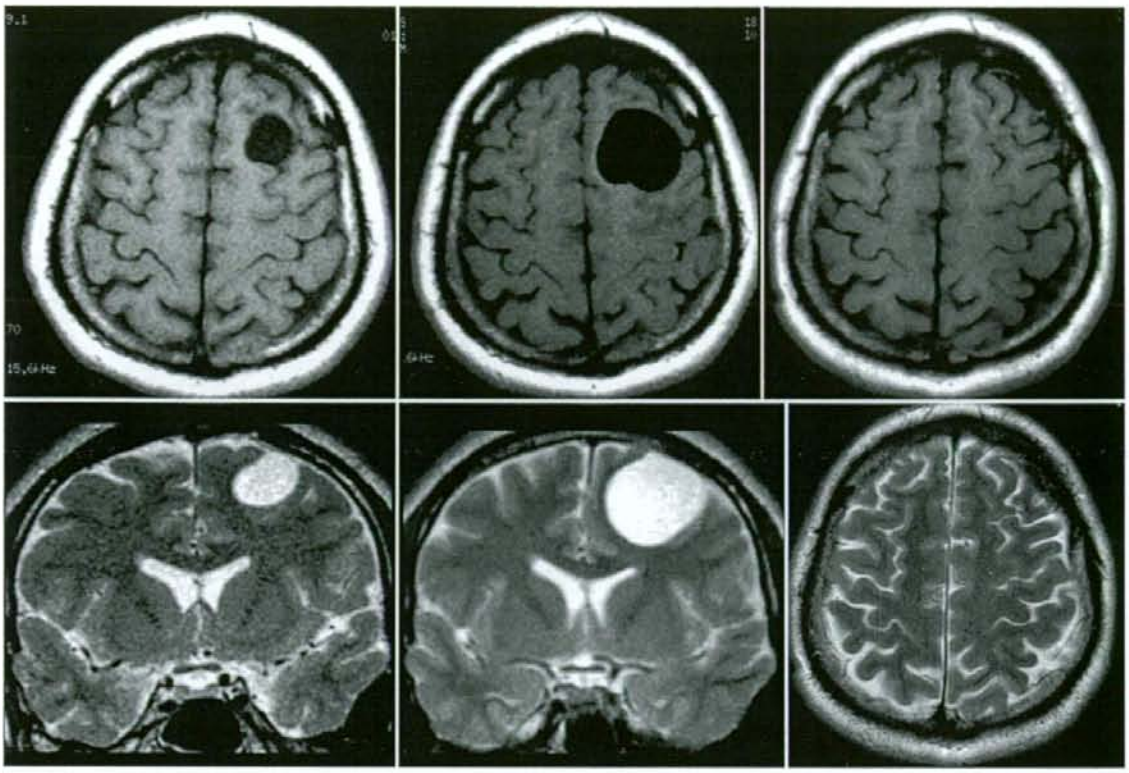

Fig. 1. Axial postcontrast T_1-weighted (*upper left*) and coronal T_2-weighted (*lower left*) magnetic resonance (MR) images show an extra-axial cystic mass without enhancement. Both images show that the cyst fluid was isointense to the cerebrospinal fluid (CSF). The cyst was 20 mm × 17 mm × 20 mm in size. Follow-up axial postcontrast T_1-weighted (*upper middle*) and coronal T_2-weighted (*lower middle*) MR images were taken 13 months later. The cyst was markedly enlarged, to 32 mm × 31 mm × 32 mm. Note that the signal intensity of the cyst had changed in this study, with that of the T_1 image being slightly lower and that of the T_2 image being slightly higher than the signal intensity of CSF. Postoperative axial T_1-weighted (*upper right*) and T_2-weighted (*lower right*) MR images are also shown

hyperhomogeneous signal intensity that was not enhanced by contrast medium (Fig. 1, upper left and lower left). CT scan showed no thinning of the calvarium beneath the cyst. The symptoms were easily controlled with nonsteroidal antiinflammatory drugs. After discussion with the patient and his family, no further measure was taken at that time. The follow-up MRI was scheduled for 6 months after his first visit to our clinic. The patient, however, did not visit our clinic until a year later. He complained of recent worsening of his headache. The second MRI, taken 13 months after the initial visit, showed marked expansion of the mass (Fig. 1, upper middle and lower middle), with a slightly lower intensity on the T_1 image and a slightly higher intensity on the T_2 image, compared with cerebrospinal fluid (CSF). This time, surgery was recommended, but the patient again refused any surgical procedure. Two months later, he suddenly fell with an epileptic attack, and he was admitted to our ward. Several antiepileptic drugs, including phenytoin 250 mg per day and zonisamide 400 mg per day, were administered, but the number and duration of seizures increased despite the ideal blood concentration of those drugs having been attained. On the 7th day from the first attack, he went into epileptic status, and he underwent surgery on the same day.

A craniotomy was done and the dura matter was incised; a milky-yellowish cystic bulging lesion, which had no obvious communication with other CSF spaces, was observed. The cyst wall was excised and removed. The yellowish-opaque gelatinous liquid content and the cyst wall were subjected to cytological and pathological studies, respectively.

The cytological study revealed the prevalence of clusters of pilocytic epithelium with column-like and cubic cells. No atypical or tumor-like growth was observed. Microscopic images of the cyst wall depicted a single layer to several layers of ependymal cells with cilia that lined the inner side of the wall (Fig. 2). There were neither mitoses nor signs of malignancy. Immunohistochemistry showed cytokeratin (++) and epithelial membrane antigen (EMA) (+) in the epithelium; the epithelium and basic fiber layer were negative for glial fibrillary acidic protein (GFAP) (Fig. 3). Based on these findings, we diagnosed the lesion as a neurenteric cyst.

The epileptic status completely disappeared postoperatively. The postoperative MRI taken 2 years later did not

show any recurrent sign of the cystic components. The patient is now free of symptoms and has not required the antiepileptic drugs for 32 months. The series of EEG obtained during the follow-up period have not shown any spikes or epileptogenicity.

Discussion

Supratentorial neurenteric cyst is a rare clinical entity. Its imaging spectrum is broader than considered so far,[2] as well as its location; the lesion has been found in the frontal lobe,[2-8] parietal region,[9] lateral supratentorial region,[10] and frontoparietal region.[11] Several other supratentorial lesions involved the septum pellucidum,[12] oculomotor nerve,[13,14] anterior cranial fossa,[15] and parasellar region,[16] but other CNS neurenteric cysts are located in the infratentorial or spinal region.[2]

Kim et al. reported enlargement of the lesion even at 4 years of follow-up as a developmental lesion.[17] The expansility of a neurenteric cyst is rarely reported, as these lesions have been directly subjected to surgery rather than to observation. This expansility feature is frequently observed in arachnoid cysts.[18] In most cases of supratentorial neurenteric cyst, the content was described as a viscous/gelatinous fluid of different colors,[5,8,19] reflecting various sequential changes of the protein content. Enlargement of a neurenteric cyst may result from changes in protein content composition and concentration, which is reflected in MRI signal alterations,[20] as in our patient.

The association of epileptogenicity to the neurenteric cyst in the cerebral cortex should be emphasized. Including the present case, 17 supratentorial neurenteric cysts have been reported to date. Of them, detailed clinical features are available for 14 cases, and these were used for further investigation of epileptogenesis (Table 1).

Of the 14 supratentorial neurenteric cysts observed in the frontal or parietal convexity, 9 (64%) were associated with presurgical seizures and 3 others with postsurgical seizures. Thus, in 86% (12 of 14 cases) of the patients, the lesion was involved in the occurrence of epilepsy in the perioperative period. In our patient, seizure occurred 15 months after the first evaluation, suggesting that patients without seizures might suffer epileptic seizures later on.

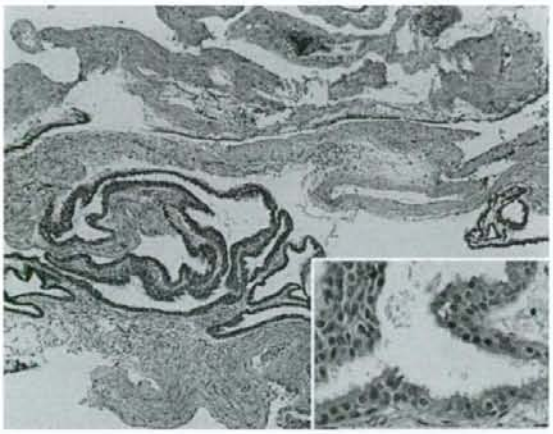

Fig. 2. The cyst wall was composed of a fibrous capsule and the lumen was covered with ciliated epithelium. There were no goblet cells. Hematoxylin and eosin (H&E) stain

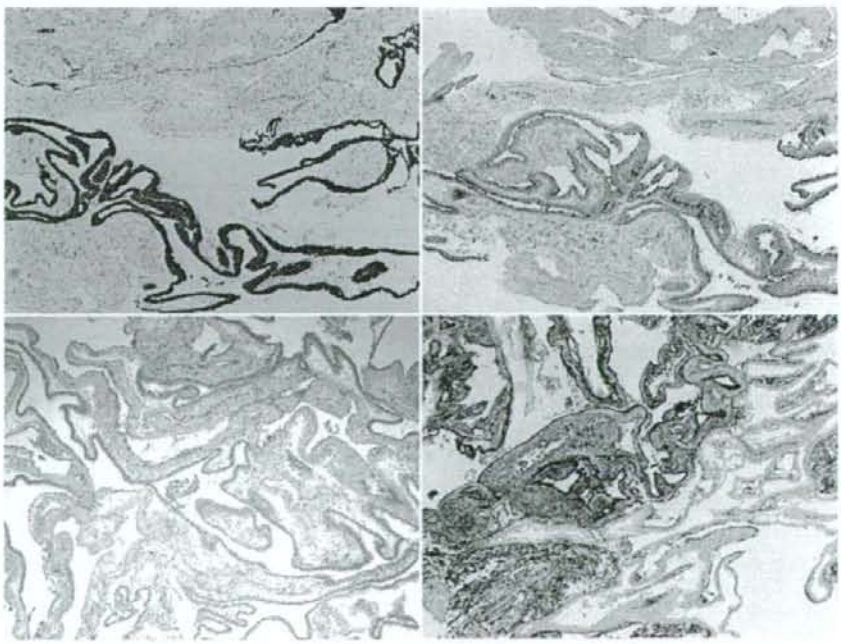

Fig. 3. Micrographs showing the results of immunohistochemistry. The epithelium of the inner wall stained strongly positive for cytokeratin (CK). The epithelium of the inner wall was positive for epithelial membrane antigen (EMA) in the film and cilia of the epithelium surface. Staining for glial fibrillary acidic protein (GFAP) was negative, but the capsule and basal membrane stained strongly positive for vimentin

Table 1. Supratentorial neurenteric cyst and epilepsy

Series (reference number, year)	Age (years)	Sex	Location	Presurgical epilepsy	Surgery	Outcome
Bavetta et al.[5] (1996)	28	M	Right frontal lobe	Two grand mal seizures	Fluid marsupialized, contents evacuated	On anticonvulsants
Ho et al.[9] (1998)	45	F	Right parietal lesion	Abrupt onset of focal sensory seizures	Gross total resection, later second surgery	
Asamoto et al.[3] (1999)	69	M	Left frontal lobe	None	Total resection	No deficit
Cheng et al.[10] (2002)	49	M	Right frontal convexity	None	Membrane removal	Two episodes of seizure activity on the third day
Suri et al.[7] (2002)	33	M	Left frontal region	No history of convulsions	Decompression and excision of cyst wall	
Christov et al.[11] (2004)	31	F	Right frontal convexity	Not described	Fluid evacuation, subsequent total removal	Postsurgical seizures, intensive long-term antiepileptic treatment
Tan et al.[8] (2004)	68	F	Left frontal convexity	Two tonic-clonic seizures affecting all four limbs and lasting for a few minutes	Aspiration	
Kachur et al.[6] (2004)	35	F	Right frontal lobe	One-year history of headache and seizure-like episodes	Excision	Improved
Stubenvoll et al.[4] (2006)	25	M	Right frontal convexity	Single, generalized tonic-clonic seizure	Cyst fenestration	Generalized seizures 5 days after surgery, no additional seizure at 3 months follow-up, discontinued anticonvulsive therapy
Preece et al.[2] (2006)	34	M	Left of midline, adjacent to calvarium, extending through left ethnoid	New-onset seizures		
Preece et al.[2] (2006)	78	F	Right frontal lobe, extraaxial	Acute-onset single seizure		
Preece et al.[2] (2006)	78	M	Frontal lobe, extraaxial	New-onset seizures		
Miyagi and Katayama[19] (2007)	63	M	Right parietal convexity	None	Parightial resection	Status epilepticus on the second postoperative day, later controlled with anticonvulsants
Our case	34	M	Left frontal convexity	Status epilepticus	Excision	Good control without AED

Status epilepticus was observed in our patient before surgery and in another patient after the operation. Status epilepticus has also been reported in patients with a neuroepithelial cyst,[21] but very rarely in those with an arachnoid cyst.[22]

At surgery, total excision with preservation of neurological function should be the goal.[23] Recurrence of neurenteric cysts has been reported together with malignant transformation after total resection,[24] or with extensive craniospinal dissemination.[25] Another reported malignancy is papillary adenocarcinoma in an enterogenous cyst.[9] As for surgical intervention of lesions that may undergo malignant transformation or dissemination, total cystectomy is indicated instead of a peritoneal shunt to prevent migrating spread of neurenteric cells into the peritoneal space. Diagnosis is made at, or even after, surgical intervention. In patients with an arachnoid cyst, a cyst–peritoneal shunt is occasionally selected,[26] but when a neurenteric cyst is presumed, shunt surgery should be avoided.

References

1. Hirano A, Hirano M (2004) Benign cysts in the central nervous system: neuropathological observations of the cyst walls. Neuropathology 24:1–7
2. Preece MT, Osborn AG, Chin SS, Smirniotopoulos JG (2006) Intracranial neurenteric cysts: imaging and pathology spectrum. AJNR Am J Neuroradiol 27:1211–1216
3. Asamoto S, Sugiyama H, Doi H, et al. (1999) A case of neuroaxis endodermal cyst. No To Shinkei 51:520–523
4. Stubenvoll F, Beschorner R, Danz S, Freudenstein D (2006) Fronto-laterally located supratentorial bronchogenic cyst: case report and review of the literature. Clin Neuropathol 25:123–127
5. Bavetta S, El-Shunnar K, Hamlyn PJ (1996) Neurenteric cyst of the anterior cranial fossa. Br J Neurosurg 10:225–227
6. Kachur E, Ang LC, Megyesi JF (2004) Intraparenchymal supratentorial neurenteric cyst. Can J Neurol Sci 31:412–416
7. Suri VS, Tatke M, Sinha S (2002) Intracranial neurenteric cysts: a report of two cases. Br J Neurosurg 16:185–188
8. Tan GS, Hortobagyi T, Al-Sarraj S, Connor SE (2004) Intracranial laterally based supratentorial neurenteric cyst. Br J Radiol 77:963–965

9. Ho LC, Olivi A, Cho CH, et al (1998) Well-differentiated papillary adenocarcinoma arising in a supratentorial enterogenous cyst: case report. Neurosurgery 43:1474–1477
10. Cheng JS, Cusick JF, Ho KC, Ulmer JL (2002) Lateral supratentorial endodermal cyst: case report and review of literature. Neurosurgery 51:493–499; discussion 499
11. Christov C, Chretien F, Brugieres P, Djindjian M (2004) Giant supratentorial enterogenous cyst: report of a case, literature review, and discussion of pathogenesis. Neurosurgery 54:759–763; discussion 763
12. Mishra GP, Sharma RR, Musa MM, Pawar SJ (2000) Endodermal cyst of septum pellucidum and pregnancy: a case report. Surg Neurol 53:583–585
13. Morgan MA, Enterline DS, Fukushima T, et al (2001) Endodermal cyst of the oculomotor nerve. Neuroradiology 43:1063–1066
14. Werner M, Bhatti MT, Vaishnav H, et al (2005) Isolated anisocoria from an endodermal cyst of the third cranial nerve mimicking an Adie's tonic pupil. J Pediatr Ophthalmol Strabismus 42:176–179
15. Neckrysh S, Valyi-Nagy T, Charbel FT (2006) Neuroenteric cyst of the anterior cranial fossa: case report and review of the literature. Surg Neurol 65:174–177; discussion 177
16. Sampath S, Yasha TC, Shetty S, Chandramouli BA (1999) Parasellar neurenteric cyst: unusual site and histology: case report. Neurosurgery 44:1335–1337; discussion 1337–1338
17. Kim CY, Wang KC, Choe G, et al (1999) Neurenteric cyst: its various presentations. Childs Nerv Syst 15:333–341
18. Basaldella L, Orvieto E, Dei Tos AP, et al (2007) Causes of arachnoid cyst development and expansion. Neurosurg Focus 22:E4
19. Miyagi A, Katayama Y (2007) Neurenteric cyst arising in the high convexity parietal lesion: case report. Neurosurgery 60:E203–E204; discussion E2044
20. Shakudo M, Inoue Y, Ohata K, Tanaka S (2001) Neurenteric cyst with alteration of signal intensity on follow-up MR images. AJNR Am J Neuroradiol 22:496–498
21. Efkan CM, Attar A, Ekinci C, Erdogan A (2000) Neuroepithelial (colloid) cyst of the parietal convexity. Acta Neurochir (Wien) 142:1167–1168
22. Jirsch JD, Andermann F, Gross DW (2002) Status epilepticus presenting in a patient with neurosyphilis and a previously asymptomatic arachnoid cyst. Epilepsia 43:775–776
23. Bejjani GK, Wright DC, Schessel D, Sekhar LN (1998) Endodermal cysts of the posterior fossa. Report of three cases and review of the literature. J Neurosurg 89:326–335
24. Sahara Y, Nagasaka T, Takayasu M, et al (2001) Recurrence of a neurenteric cyst with malignant transformation in the foramen magnum after total resection. Case report. J Neurosurg 95: 341–345
25. Kimura H, Nagatomi A, Ochi M, Kurisu K (2006) Intracranial neurenteric cyst with recurrence and extensive craniospinal dissemination. Acta Neurochir (Wien) 148:347–352; discussion 352
26. Pradilla G, Jallo G (2007) Arachnoid cysts: case series and review of the literature. Neurosurg Focus 22:E7

Childs Nerv Syst (2008) 24:927–932
DOI 10.1007/s00381-007-0574-4

ORIGINAL PAPER

Catcher's mask cranioplasty for extensive cranial defects in children with an open head trauma: a novel application of partial cranioplasty

Ichiro Takumi · Masataka Akimoto

Received: 17 November 2007 / Published online: 29 January 2008

Abstract
Objective In children who have suffered a severe, extensive head trauma, cranioplasty is complicated because allografting is not advisable in pediatric patients and the amount of available autologous materials is limited. To overcome these problems, we employed a combination of autologous rib grafts and calvarial grafts for partial cranioplasty.
Materials and methods We named this partial cranioplasty technique 'catcher's mask cranioplasty'. Rib grafts were placed mimicking a baseball catcher's mask to obtain maximum strong coverage of the defect. Calvarial grafts were used to achieve a smooth forehead contour. Islands of osteoanagenesis were also used.
Conclusions These autografts were of sufficient strength, esthetically satisfactory, and no patient developed sinking skin flap syndrome. Catcher's mask cranioplasty is a useful technique to successfully reconstruct the skull in pediatric patients with extensive cranial defects and an insufficient amount of autologous graft material.

Keywords Huge cranial defect · Catcher's mask · Rib graft · Calvarial graft · Partial cranioplasty

Introduction

In patients for whom external decompression is required, cranioplasty is usually performed using their own skull. Although the interval between the 1st and 2nd operation varies [12], frozen [12], frozen and autoclaved [19], or subcutaneously preserved [20] autologous skull is most commonly used for cranioplasty. Some cases are complicated by the presence of a contaminated wound or post-surgical infection of the cranioplasty and require another intervention. Although a salvage method has been reported to treat patients with post-craniotomy infection [2], the infected bone flap is usually removed. On the other hand, when the splinter of the skull itself is severely contaminated, with or without laceration of the dura matter, such as in the case of a complex open skull injury, the autologous skull is not preserved at the time of trauma surgery.

Allograft and autologous grafts are the options for cranioplasty. Reported allograft materials are polymethylmethacrylate (PMMA) [4, 19], hydroxyapatite (HA) [19, 22], and titanium [13, 19]; a tissue engineering method [5] has even been suggested. Although some children have undergone allograft cranioplasty [4], the use of autogenic material is preferred [7, 30, 13, 25]. In autologous cranioplasty, either rib grafts or calvarial grafts have been used for years. The more modern techniques were introduced by Tessier and Tessier et al. in the 1980s [26, 28]. While autologous grafts are advantageous in infancy and reduce the risk of infections, the amount of available autologous material is usually insufficient, especially in patients with huge defects.

All the current cranioplasty techniques are based on the 'full coverage cranioplasty' principle, that is, the whole defect is covered. Here, we present a novel technique for 'partial cranioplasty' that overcomes the aforementioned problems. This is a combined method that involves split-rib and split-calvarial grafting in the shape of a catcher's mask, which we devised to cover a huge postoperative skull defect with ease, partly by crossing those grafts. Islands of

I. Takumi · M. Akimoto (✉)
NMS Cranio-Facial Institute,
Nippon Medical School Chiba Hokuso Hospital,
1715 Kamagari, Inba-gun Inba-mura,
Chiba Hokuso 270-1694, Japan
e-mail: akimoto@nms.ac.jp

osteoanagenesis are also used. Our method proved to be safe and effective.

Materials and methods

The patients were three children with extensive open head trauma. All of them presented with traumatic brain protrusion from the wound and underwent external decompression. Their skulls were not preserved because these were severely contaminated or even drilled out at injury. Cranioplasty was performed 6–12 months after the injury. Rib grafts were harvested from the 7th and/or 9th rib. The ribs were removed in toto or split in half in situ. Calvarial grafts were harvested in situ from the outer layer of the calvarium while leaving the inner skull layer intact. The rib grafts were placed across each other mimicking a baseball catcher's mask, providing thereby a sound foundation that required minimal grafting material, and a 3-D dynamic base. For fixation, we used either surgical steel (DS-28, Ethicon, Somerville, NJ, USA) or nylon thread. Calvarial grafts were placed to shape the forehead and attempts were made to decrease the likelihood of graft resorption and desorption of the forehead. Islands of osteoanagenesis were used to shape the cranium. As our cranioplasty technique is reminiscent of a baseball catcher's mask, we named it "catcher's mask cranioplasty".

Results

Patient 1

This 9-year-old boy was brought to our emergency room after his head was crushed by a tractor. On admission, his consciousness level was E2M2V2 on the Glasgow coma scale (GCS); he had left hemiparesis and the brain protruded from the wound. Computed tomography (CT) revealed acute subdural hematoma, open depressed skull fracture, pneumocephalus, cerebral contusion, and brain protrusion from the wound. He was operated on immediately. At surgery, there was massive damage to the skull, dura mater, and brain parenchyma. The open fracture crossed the midline. We performed a large right-side frontotemporal craniotomy and external decompression for intracranial pressure control. As the skull was contaminated by dirt and oil in areas on the left of the midline, craniotomy was expanded to the contralateral side. Minimal local lobectomy was performed for debridement. The dirty dura mater was resected and a large patch was placed using free fascia lata. Contamination prevented preservation of the craniectomized skull bone.

Eight months later, he underwent cranioplasty. The defect measured 162 cm^2. The rib grafts were harvested from the right 7th and 9th ribs. The entire 9th rib was harvested and split for grafting. The 7th rib was split in situ, one half was used for grafting and the other half was left in place. Only the outer layer of the skull was harvested and used as a calvarial graft; it was harvested from an area inside the hairline. The graft materials derived from the skull and ribs were combined to create a cranioplasty in the shape of a catcher's mask (Fig. 1).

Postoperative 3-D CT scans obtained 37 months later are shown in Fig. 2 (left). The 3-D framework remained stable for 5 years after grafting, and the patient was able to undergo rehabilitation. The result was cosmetically satisfactory (Fig. 3) and MRI indicated no sinking flap syndrome despite contusional changes (Fig. 2, right). The 99mTc-HMDP SPECT study performed at 37 months confirmed that the graft had taken up well.

At the time of this report, 5 years have passed since the catcher's mask cranioplasty surgery. The patient manifests no motor deficits or mental retardation and is able to pursue an almost normal life at school being able to engage in swimming and other sports activities.

Patient 2

This 6-year-old boy was brought to our emergency room after a serious traffic accident. On admission, his con-

Fig. 1 Patient 1—catcher's mask cranioplasty. Photograph showing the calvarial graft placed on the forehead. The rib grafts are placed across each other mimicking a catcher's mask (*left*). The 3-D CT scan (*right*) was taken 10 days after the operation

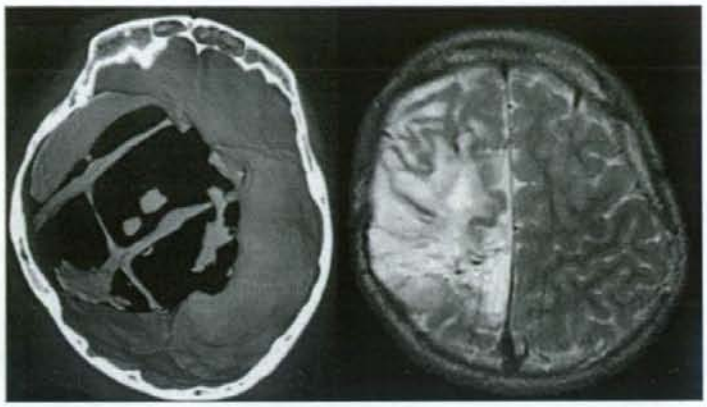

Fig. 2 Patient 1—3-D CT scans taken 37 months after the catcher's mask cranioplasty (*left*). Note that the rib grafts continue to provide a strong 3-D foundation. The calvarial forehead graft is well preserved. The areas of osteoanagenesis had expanded. The T2-weighted MRI scan shows excellent 3-D construction without sinking flap syndrome (*right*)

sciousness level was E1M2V4 on the GCS; he had right hemiparesis, a large open forehead wound, marked laceration of the dura mater, and the brain protruded from the wound. Initial trauma investigation revealed an open depressed skull fracture with bone migration into the brain parenchyma, pneumocephalus, cerebral contusion, and brain protrusion from the wound. He was operated on immediately. His skull was not preserved because of the presence of dirt. Twelve months after the acute-phase surgery, he underwent catcher's mask cranioplasty. The defect measured 144 cm^2. As shown in Fig. 4, there were widespread areas of osteoanagenesis at the time of surgery, and these were used to shape the skull.

The follow-up examination 37 months after the cranioplasty showed successful cranial protection, and the patient is now able to undergo rehabilitation without wearing head protection.

Patient 3

This 8-year-old boy was taken to a regional trauma care center after a serious traffic accident. He had been hit and dragged by a freight car. His occipital was totally injured, his scalp and dura matter were lacerated, with his skull shaved off and absent. The contused brain was directly seen from the wound. On admission, his consciousness level was E1M2V5 on the GCS. His skull was not preserved because it had partly disappeared. He was well treated at the trauma center and was referred to our institute 4 months after the traffic accident. On admission, he only presented homonymous hemianopia. We performed the catcher's mask cranioplasty 6 months after the traffic accident (Fig. 5). The huge defect was covered with crossed ribs, but the coverage was designed only to cover the supratentorial defects, as the infratentorial portion had already started to

Fig. 3 Patient 1—photographs showing the excellent cosmetic outcome